

Ionotronics Based on Horizontally Aligned Carbon Nanotubes

Ran Peng, Yueyue Pan, Zhi Li, Shuailong Zhang, Aaron R. Wheeler, Xiaowu (Shirley) Tang, and Xinyu Liu*

Controlled ion transport through ion channels of cell membranes regulates signal transduction processes in biological systems and has also inspired the thriving development of ionic electronics (ionotronics or iontronics) and biocomputing. However, for constructing highly integrated ionic electronic circuits, the integration of natural membrane-spanning ion channel proteins or artificial nanomembrane-based ionic diodes into planar chips is still challenging due to the vertically arranged architecture of conventional nanomembrane-based artificial ionic diodes. Here, a new design of ionic diode is reported, which allows chip-scale integration of ionotronics, based on horizontally aligned nanochannels made from multiwalled carbon nanotubes (MWCNTs). The rectification of ion transport through the MWCNT nanochannels is enabled by decoration of oppositely charged polyelectrolytes on the channel entrances. Advanced ionic electronic circuits including ionic logic gates, ionic current rectifiers, and ionic bipolar junction transistors (IBJT) are demonstrated on planar nanofluidic chips by stacking a series of ionic diodes fabricated from the same bundles of MWCNTs. The horizontal arrangement and facile chip-scale fabrication of the MWCNT ionic diodes may enable new designs of complex but monolithic ionotronic systems. The MWCNT ionic diode may also prove to be an excellent platform for investigation of electrokinetic ion transport in 1D carbon materials.

1. Introduction

Electrokinetic regulation of ion transport through ion channels in biological systems is essential to a variety of cellular mechanisms and activities,^[1–3] and has attracted increasing research efforts on developing bioinspired ion-flow regulation devices such as ionic diodes and transistors to mimic controlled ion transport in biological ion channels.^[4–8] These ionic devices have found significant applications in logic computing,^[9–12] sensing,^[13,14] energy conversion,^[15,16] to name just a few. Natural or synthetic biological ion channels could serve as ideal building blocks for constructing ionic devices due to their atomic pore sizes and self-organized polyelectrolyte-based functional structures.^[17–20] However, these biological ion channels are mechanically fragile and chemically sensitive, making it challenging to integrate them with engineering devices.^[21] Leveraging material science and nanotechnology approaches, various nanochannels, nanopores and nanomembranes, constructed from solid-state materials or polymers, have

been developed to act as ion-flow regulation confinements with high mechanical robustness and structural controllability. The controlled regulation of ion transport through these nanoscale confinements has been achieved via surface functionalization of the nanostructures with charged molecular groups.^[1,22–23]

The commonly used membrane-based artificial ion nanochannels spanning the membrane thickness are low in aspect ratio; thus, it is not feasible for asymmetric surface functionalization with opposite charges due to the crosstalk of modification fluids during wet modification.^[24] On the other hand, wafer-scale batch fabrication of ionic diodes made from horizontally aligned nanochannels of sub-10 nm in diameter is still technically challenging.^[25] More importantly, because of the less effective charge modification on membrane-based short ionic nanochannels and the relatively large channel diameters of nanochannel-based ionic tunnels, the reported ionic diodes usually have limited current rectification ratios, which are not applicable for certain applications such as ionic circuits for logic computing.^[9–12] In addition, the integration of these membrane-spanning, vertically aligned (perpendicular to the membrane plane) ion nanochannels into on-chip ionic circuits that mimic their traditional electronic counterparts is highly challenging because of the poor compatibility between the in-plane arranged ionic circuit architecture and the vertical


Dr. R. Peng, Y. Pan, Prof. X. Liu
Department of Mechanical and Industrial Engineering
University of Toronto
5 King's College Road, Toronto, ON M5S 3G8, Canada
E-mail: xyliu@mie.utoronto.ca

Z. Li, Prof. X. Tang
Department of Chemistry & Waterloo Institute
for Nanotechnology (WIN)
University of Waterloo
200 University Avenue West, Waterloo, ON N2L 3G1, Canada

Dr. S. Zhang, Prof. A. R. Wheeler
Department of Chemistry
University of Toronto
Toronto, ON M5S 3H6, Canada

Dr. S. Zhang, Prof. A. R. Wheeler, Prof. X. Liu
Institute of Biomaterials and Biomedical Engineering
University of Toronto
164 College Street, Toronto, ON M5S 3G9, Canada

Dr. S. Zhang, Prof. A. R. Wheeler
Donnelly Centre for Cellular and Biomolecular Research
University of Toronto
160 College Street, Toronto, ON M5S 3E1, Canada

 The ORCID identification number(s) for the author(s) of this article can be found under <https://doi.org/10.1002/adfm.202003177>.

DOI: 10.1002/adfm.202003177

(out-of-plane) alignment of the membrane-based nanochannels. As a result, there have been just a few reports of integrated on-chip ionic logic gates, rectifiers and transistors that involve multiple ionic diodes.^[10,26] It is therefore highly desired to develop new ionic diode architectures with easy-to-fabricate, in-plane nanochannel structures compatible with wafer-scale batch fabrication process, which could enable new applications where integrated ionic circuits are needed.

Advances in the integrated circuit (IC) industry highlight the great promise of carbon nanotubes (CNTs) as an electronic channel material due to their nanometer diameters and superior charge transport properties over silicon (Si).^[27,28] Recent breakthroughs on nanofabrication and large-scale integration of CNT-based transistors also confirmed the material's compatibility with wafer-scale fabrication processes, and solved the bottleneck issues of CNT-based electronics moving towards practical uses.^[29–31] For fluid and ion transport, the nanotubular structure of CNTs can also serve as high-performance artificial ionic nanochannels.^[32,33] Previous studies have demonstrated that fluid and ion transport in CNT nanochannels is ultra-efficient,^[32,34] which could potentially improve the performance of ionotronics. Also, the atomic inner diameter of CNTs is advantageous to mimic natural biological ion channels with similar pore sizes,^[35] and the ultralong channel length of CNTs is beneficial for asymmetric modification of charges as well as integration of horizontally aligned chip-scale ionic circuits. Charge modification of CNT-based nanochannels can be readily conducted on the CNT terminals using well-established techniques.^[36] There have been several studies on controlled ion transport in CNT nanochannels;^[37–40] however, little effort has been spent on design and batch fabrication of CNT-based ionic diodes and exploration of their applications on ionic circuits.

In this paper, we report the design and batch fabrication of a novel CNT-based ionic diode with horizontally aligned polyelectrolyte-modified multiwalled CNTs (MWCNTs) serving as ion channels. The two openings of MWCNTs are decorated with oppositely charged polyelectrolytes through strong physical absorption on the active carbon sites at the MWCNT terminal edges. The rectification of ionic current is governed by asymmetric transport of ions through the MWCNT nanochannels due to the oppositely charged terminals. The design and working parameters of the MWCNT ionic diode are systematically investigated, and the diode performance is evaluated by the ionic current rectification ratio with a specific voltage scanning range. Enabled by the new batch fabrication process, multiple MWCNT ionic diodes are integrated on single nanofluidic chips to realize ionic logic gates, ionic rectifiers, and ionic bipolar junction transistors (IBJT), which promises high potential of our MWCNT ionic diode for constructing monolithic ionotronic systems with many diode and transistor components.

2. Results and Discussion

2.1. Design and Fabrication of MWCNT Ionic Diodes and Setup of Experimental Systems

Current rectification in ionic diodes, similar to that in semiconductor diodes, is based on the generation of an accumulation

or depletion region of ions in a nanochannel with asymmetric geometry or surface properties (surface charge or wettability) during diode operation.^[2,3,41] However, in an ionic diode, cations and anions are employed as charge carriers rather than electrons and holes in its semiconductor counterpart. The MWCNT ionic diode we propose here falls into the category of bipolar ionic diodes with asymmetric charges labelled on two terminals of the MWCNT nanochannel. **Figure 1a,b** illustrate the architecture and the working principle of a MWCNT ionic diode, respectively. As shown in **Figure 1a**, a group of well-aligned MWCNTs serve as ionic nanochannels that bridge two microchannels filled with KCl electrolytes mixed with polycations, poly(diallyldimethylammonium chloride) (PDAC) and polyanions, poly(sodium 4-styrene-sulfonate) (PSS), respectively. An electric field is applied to the MWCNT nanochannels, through the upstream and downstream microchannels, to drive the mobile ions. The active carbon sites on the two terminals of each MWCNT are capable of immobilizing positively charged long polyelectrolyte chains on one side and negatively charged ones on the other side via physical absorption,^[42–45] as illustrated in **Figure 1b**. As a result, when a forward or reverse electric field is applied on the MWCNT channel, the mobile K⁺ and Cl[−] ions get accumulated (top schematic in **Figure 1b**) or depleted (bottom schematic in **Figure 1b**) inside the MWCNT nanochannel, respectively. This ion accumulation/depletion effect is due to the electrostatic attraction or repulsion between the mobile ions and the charged groups on the long polyelectrolyte chains immobilized at the two terminals of the MWCNT. These phenomena induce the enhancement or reduction of the overall electric conductivity of the MWCNT ion channel and thus lead to the ionic diode effect.

Although the ionic diode effect of CNT nanochannels has been reported previously,^[37–40] the device-level application of CNT-based ionic diodes for ionotronics is rarely explored because of the technical challenges on device fabrication such as synthesis, isolation, and alignment of long CNTs and precise patterning and integration of multiple CNT nanochannels into a microfluidic device.^[46] Herein, we propose a facile approach to integrate horizontally aligned MWCNT nanochannels into a microfluidic device with accurate control of their positions and lengths. To start the device fabrication, vertically aligned MWCNT forests with a height of around 500 μm (**Figure 1c**) were first synthesized through chemical vapor deposition (CVD)^[47] on a Si wafer. **Figure 1d** shows a zoomed-in view of the top edge of the highly aligned MWCNT forest. The inset of **Figure 1d** plots the inner diameter distribution of the MWCNTs with an average of 5 nm, which was measured by a high-resolution transmission electron microscope (TEM) (**Figure S2i**, Supporting Information). Then, the vertically aligned MWCNT forests were laid down to their growth substrate, exfoliated into a thin horizontally aligned MWCNT bundle by a Scotch tape (**Figure 1e**).^[21] After that, the MWCNT nanofluidic device was fabricated by following the process shown in **Figure 1f**. Briefly, the exfoliated MWCNT bundle was first transferred onto a Si wafer (coated with a 300 nm thick SiO₂ insulation layer) and embedded in photoresist by spin coating (**Figure 1f-I**). The two microchannels were then transferred onto the substrate by exposing the sample to UV light through a photomask (**Figure 1f-II**). After development of the

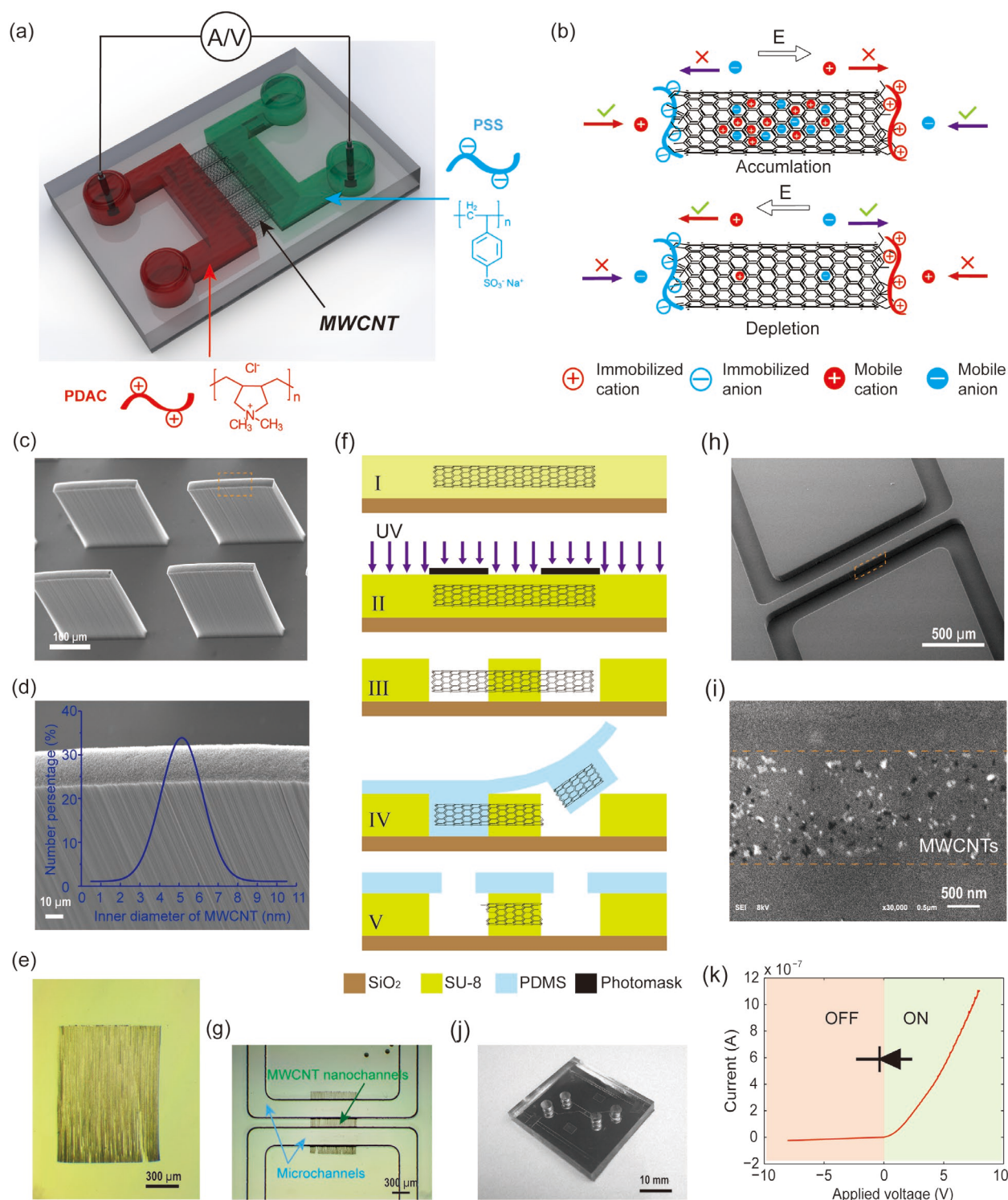


Figure 1. Design, fabrication, and characterization of the MWCNT ionic diode. a) Schematic of a MWCNT ionic diode filled with polyelectrolyte solutions (PSS and PDAC) and configuration of the electrical measurement system. b) Schematic working principle of the MWCNT ionic diode. c) SEM image of four vertically aligned MWCNT forests. d) Zoomed-in SEM image of a MWCNT forest. The inset of (d) plots the distribution of the MWCNT inner diameter. e) An optical image of a MWCNT array exfoliated by Scotch tape. f) Fabrication process of the MWCNT nanofluidic device. g) Optical and h) SEM images of a MWCNT nanofluidic device after mechanical avulsion of the MWCNTs (after Step III in (f)). i) SEM image of the zoomed-in side-view of the MWCNTs embedded in the sidewall between the microfluidic channels after mechanical avulsion. The area embedded with MWCNTs is framed within the two dashed lines. j) Photograph of the MWCNT nanofluidic device after plasma-assisted bonding of the PDMS roof layer. k) An example current-voltage (I-V) curve measured from a MWCNT ionic diode with apparent "ON" and "OFF" status with an ionic current rectification ratio of 36.1 at ± 5 V.

unexposed area, two microchannels were created and the two terminals of the embedded MWCNTs were exposed inside the microchannels (Figure 1f-III). Cutting and opening of the MWCNTs were conducted by casting PDMS precursor into the microchannels followed by mechanical avulsion of the thermally cured PDMS elastomer (Figure 1f-IV). The final chip was obtained by plasma-assisted bonding a piece of PDMS cover punched with channel reservoirs onto the nanofluidic platform (Figure 1f-V). Figure 1g,h illustrate images of a nanofluidic chip after avulsion of the MWCNTs, in which two microchannels are bridged by a bundle of MWCNT nanochannels. The vacant microchannels shown in Figure 1g,h suggest that the mechanical avulsion method is able to successfully cut MWCNTs with high efficiency.

We also tried the previously reported oxygen plasma etching method,^[48] and found that our mechanical avulsion method is easier to implement and provides much cleaner cutting of the MWCNTs than the oxygen plasma etching method (Figure S2l,m, Supporting Information). A zoomed-in scanning electron microscopic (SEM) image (Figure 1i) of the sidewall of the SU-8 sidewall between the two microchannels (Figure 1h) shows the cleanly cut openings of the MWCNT nanochannels embedded in SU-8 sidewall, from which the thickness of the exfoliated MWCNT layer was measured to be $1.65 \pm 0.4 \mu\text{m}$ ($n = 3$). Figure 1j shows the image of a completed MWCNT nanofluidic device after PDMS roof bonding. More details about the fabrication and characterization of the MWCNT nanofluidic device can be found in Figures S2 and S3 in the Supporting Information.

For device testing, the two microchannels of a sealed MWCNT nanofluidic device were filled with KCl solutions mixed with PDAC and PSS, respectively, and linear scanning direct current (DC) electric fields were then applied between the two microchannels through platinum (Pt) electrodes (Figure 1a) to drive the charge carriers across the MWCNT ionic diode. Pt wire electrodes were applied due to their outstanding properties such as chemical inertness, high conductivity, and ease of assembly in microfluidic and nanofluidic systems. Figure 1k gives a representative current–voltage (I – V) curve obtained from a MWCNT ionic diode working under the condition of $10 \times 10^{-3} \text{ M}$ KCl solution mixed with 1% polyelectrolytes, which clearly shows the diode's "ON" and "OFF" states when a forward voltage and a reverse voltage were applied, respectively. Based on the I – V curve in Figure 1k, the forward electric current at 5 V is $0.53 \mu\text{A}$ while the reverse electric current at -5 V is only 14.7 nA , indicating a current rectification ratio of 36.1. It is worth noting that both the ion current level and the current rectification ratio differ from chip to chip due to the inconsistency in the number and quality of MWCNTs in each bundle. In the working parameter studies, for each parameter, all the experiments were performed on the same chip to avoid the inconsistency problem. To develop integrated ionic circuits, multiple ionic diodes on one chip were fabricated by using one bundle of MWCNTs in order to minimize the variation in performance from diode to diode.

The design of the MWCNT nanofluidic device also has the following merits compared with other ionic diodes with nanochannels created on polymer-based nanomembranes.^[1,22,49,50] Firstly, thanks to the strong physical interaction between the

MWCNT terminals and the polyelectrolyte molecules, the charge modification on MWCNT terminals through physical absorption is much easier and more efficient than those of ionic diodes in which complicated chemical modification processes were involved.^[1] In our design, the "pipette-and-play" mode of diode charge modification significantly reduces the incubation time and improves the preparation efficiency of the MWCNT ionic diode. Even though the physical absorption of the polyelectrolytes on the MWCNT terminals is not as strong as covalent bonding^[27] and can be affected by washing of the microchannels with KCl solutions (Figure S5a, Supporting Information), filling the microchannels with evenly dispersed polyelectrolyte–KCl solutions results in the dynamic equilibrium of polyelectrolyte absorption on the MWCNT terminals and thus the stable performance of the MWCNT ionic diode. Moreover, the high aspect ratio of MWCNT nanochannels effectively reduces crosstalk of oppositely charged polyelectrolytes from the two microchannels during charge modification of the MWCNT terminals. The ultralong MWCNT forest (Figure 1d) also allows the fabrication of horizontally aligned nanofluidic channels with well-controlled position and length through conventional photolithography. The architecture of horizontally aligned MWCNT nanochannels and the facile microfabrication make it possible to develop advanced ionotronic systems with multiple MWCNT ionic diodes integrated on a planar substrate, which could become the ionic analogue of CNT-based semiconductor transistors.

2.2. Working Principle of the MWCNT Ionic Diode

The ionic diode is one of the building blocks of the emerging ionotronics. To take advantage of the newly designed MWCNT ionic systems, one must first fully understand the working mechanism and performance of the MWCNT ionic diodes. In this paper, both numerical simulations and experimental testing are conducted to systematically study the working principle of the MWCNT ionic diode. Numerical simulations were carried out based on Poisson–Nernst–Planck equations,^[51] and detailed simulation conditions can be found in Section 1 of the Supporting Information. Note that the diode operation parameters applied in the simulation models here are not exactly the same as those in our experiments due to difficulties in characterization of some of the working parameters such as charge densities at the polyelectrolyte-modified MWCNT terminals, diameters of individual MWCNT nanochannels and length of the charge modification. Nevertheless, the simulation results are still valid to verify the working principle of the MWCNT ionic diode and qualitatively evaluate the influence of different designs and operation parameters. For instance, Figure 2a shows a numerical I – V curve through a nanochannel of 7 nm in diameter and 50 nm in length modified with $\pm 2 \text{ mC m}^{-2}$ charges on the nanochannel terminals and worked with $1 \times 10^{-3} \text{ M}$ KCl. The numerical I – V curve in Figure 2a is similar to the measured I – V curve demonstrated in Figure 1k, proving the validity of our simulation model. The insets of Figure 2a present distributions of the total ionic concentration (in neutral solution where H^+ and OH^- are negligible) inside the nanochannel when a forward bias (the "accumulation" case) and a

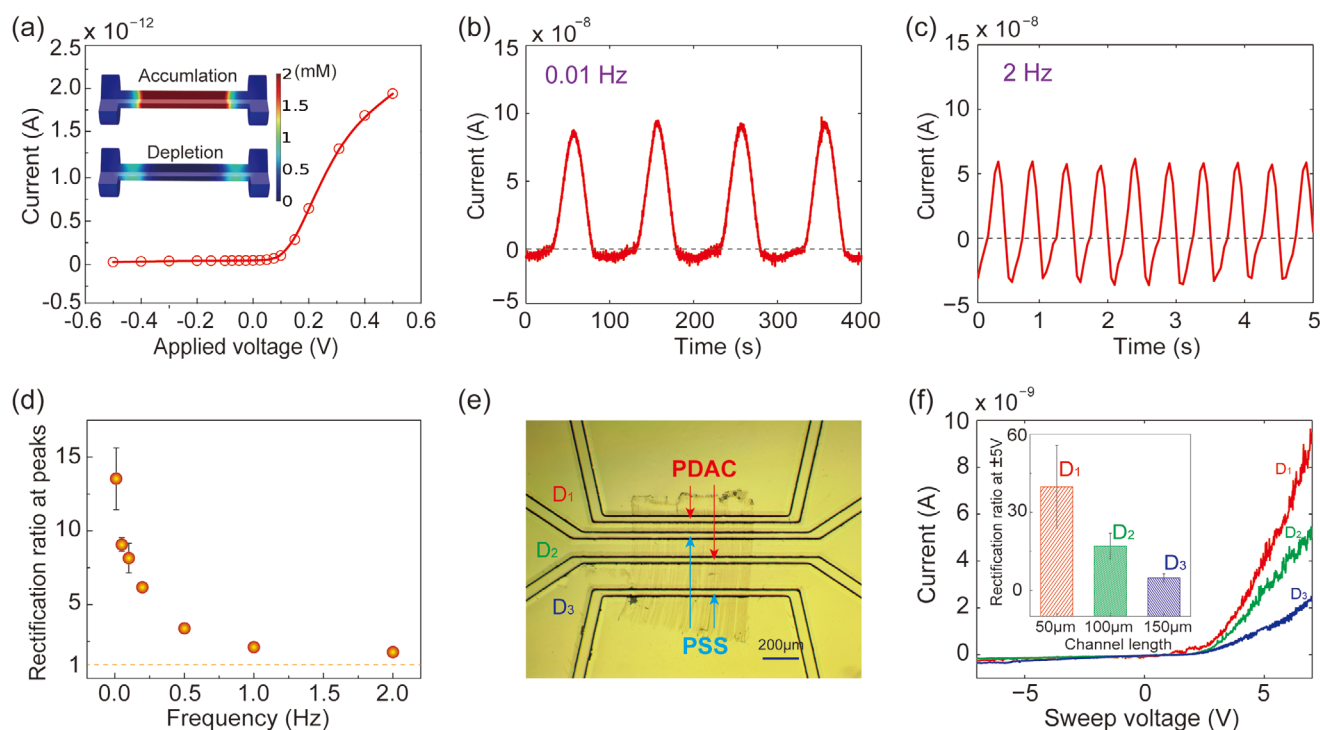


Figure 2. Performance of the MWCNT ionic diode in response to the signal frequency and the channel length. a) Numerical simulation result of the I - V characteristics of a MWCNT ionic diode. The insets illustrate accumulation and depletion of mobile ions when forward and reverse bias voltages are applied on the nanochannel. Experimental results of ionic diode currents rectified from sinusoidal input signals of b) 0.01 Hz and c) 2 Hz with an amplitude of 8 V. d) Rectification ratios (at peak amplitudes) of the ionic diode working with sinusoidal waves of different frequencies. e) Optical image of a nanofluidic chip integrated of three ionic diodes (D_1 , D_2 , and D_3) with different CNT channel lengths (50, 100, and 150 μm). These three ionic diodes were fabricated from the same bundle of MWCNTs and modified with PDAC and PSS alternatively on their terminals. f) Typical I - V curves of D_1 , D_2 , and D_3 . The inset bar chart demonstrates the corresponding rectification ratios of these three ionic diodes at ± 5 V bias voltages ($n = 5$).

reverse bias (the “depletion” case) are applied. Apparently, the mobile ions accumulate inside the channel when a forward bias is applied and deplete inside the channel when a reverse bias is applied, which verifies our proposed working principle of the MWCNT ionic diode (illustrated in Figure 1b).

Extensive confirmatory experiments have also been conducted to validate our design and to further explore the rectification behavior of the MWCNT ionic diode. For instance, with the diode characteristic, the MWCNT ionic diode should be able to rectify alternating current (AC) signals. Figure 2b shows a representative experimental rectification curve of a sinusoidal signal at 0.01 Hz generated by a MWCNT ionic diode. Rectifying square and triangular waves on the MWCNT ionic diode are also demonstrated experimentally (Figure S5b,c, Supporting Information). We also experimentally demonstrated that a MWCNT nanofluidic device without polyelectrolyte modification on the MWCNT terminals does not possess the ionic current rectification behavior, as shown in Figure S5e,f in the Supporting Information. For an ion channel with a micrometer-sized cross-section, although the upstream and downstream microchannels were filled with polyelectrolytes of opposite charges, no ionic current rectification behavior was observed experimentally (Figure S5g,h, Supporting Information). For the effect of ion channel diameter, numerical simulation results show that, with the same charge density at the ion channel terminals, the rectification ratio of the ionic diode

dramatically decreases with the channel diameter while the ion current increases with the channel diameter due to the increase of channel conductivity (Figure S5i, Supporting Information). For example, with other conditions kept the same: $\pm 2 \text{ mC m}^{-2}$ charges on the MWCNT terminals and $1 \times 10^{-3} \text{ M}$ KCl solution in the upstream and downstream channels, a nanochannel of 1 nm in diameter (assuming that the continuum condition is still valid) has a high rectification ratio of ≈ 800 (forward current: $1.23 \times 10^{-13} \text{ A}$, and reverse current: $1.69 \times 10^{-16} \text{ A}$), while a nanochannel of 30 nm in diameter has a low rectification ratio of ≈ 1.5 (forward current: $1.02 \times 10^{-11} \text{ A}$, and reverse current: $7.62 \times 10^{-12} \text{ A}$). In addition, to verify that the current rectification behavior is attributed to ion transport through the hollow nanochannels rather than inherent electrical conductivity of the MWCNTs, replacing the open-ended MWCNTs with dead-ended MWCNTs would uncover the speculation. However, it is highly challenging experimentally to fully block the ends of MWCNTs or synthesize perfect MWCNTs without any defects along the tubes. Alternatively, a conductive Pt wire without ion tunnels inside was applied to mimic dead-ended MWCNTs. The I - V behavior of a Pt wire (15 mm long and 250 μm in diameter) with its two ends immersed in PDAC and PSS solutions (Figure S5j, Supporting Information) was tested, and no current rectification phenomenon was observed (Figure S5l, Supporting Information). This indicates that merely electrically conductive channels (the scenario of WMCNT channels without

ion transport inside) cannot give rise to current rectification, and the rectification behavior is due to the controlled ion transport across the MWCNT ion channels with oppositely charged terminals. Based on the numerical and experimental results presented above, it is concluded that two necessary conditions are needed for designing high-performance MWCNT ionic diodes: a) ionic nanochannels with small enough diameters (this condition will be further discussed in the following sections) and b) modification of opposite charges on the terminals of the MWCNT nanochannels.

2.2.1. Effects of Working Frequency and Ion Channel Length

To optimize the ionic diode design, it is important to quantitatively study several other key operation parameters. Switching time is one of the most important working parameters for ionic diodes. It was reported that ionic charges in aqueous solutions respond slower to the driving electric field than their electronic counterparts (electrons and holes in semiconductor materials) by seven orders of magnitudes, which is primarily due to the viscosity of fluids and the retardation effect.^[52] As a result, ionic diodes can only work properly at relatively low frequencies.^[26] We experimentally examined the response of a MWCNT ionic diode to the frequency of sinusoidal voltage applied by a function generator in the range of 0.01 to 2 Hz with a constant magnitude of 8 V, as schematically illustrated in Figure S6a in the Supporting Information. The forward and reverse peak values of the rectified currents were used to calculate the rectification ratio of the ionic diode under different signal frequencies. Figure 2b,c show the rectified current curves recorded at 0.01 and 2 Hz, respectively. The curves at other frequencies, including 0.05, 0.1, 0.2, 0.5, and 1 Hz, are shown in Figure S6b–f in the Supporting Information. Figure 2d summarizes the rectification ratio of the MWCNT ionic diode as a function of the sinusoidal signal frequency, showing a decreasing trend of the rectification ratio from 13.5 ± 2.1 to 1.8 ± 0.1 ($n = 4$ for both) with the frequency ranging from 0.01 to 2 Hz. As mentioned above, the decrease in current rectification ratio was caused by the intrinsically slow response of the controlled ion transport in aqueous solutions.^[26,52] The frequency response range of the ionic diode could be further expanded through several methods such as shortening ion channel length, using mobile ions with higher mobility, and involving conductive polymer electrodes.^[26] Previous studies have revealed that the low-friction slip boundary of CNT inner walls would significantly enhances the fluid transport speed,^[53–55] and thus benefits the switching speed of our MWCNT ionic diode. However, based on the experimental results shown in Figure 2d and Figure S6 in the Supporting Information, one can see that the slow ion mobility in aqueous solutions dominates the switch speed of the MWCNT ionic diode and the MWCNT diode is more suitable for low-frequency applications. In addition, the operation voltage is also important to ionic diodes in some specific applications such as energy harvesting^[56,57] and wave rectification.^[26,49] During our experiments, square waves ranging from 10 to 40 V in amplitude were applied to a MWCNT ionic diode, and the ionic diode operated normally without electrical breakdown over the entire voltage range (Figure S7a–f,

Supporting Information). This suggests that our MWCNT ionic diode can reliably operate in ionotronic platforms where high operation voltages are required.

The ion channel length also significantly affects the performance of ionic diodes; however, previous research mainly focused on theoretical analysis and/or numerical simulations of the effect of ion channel length on ionic diode performance,^[58,59] and there is a lack of related experimental studies. To the best of our knowledge, we performed the first investigation of the effect of ion channel length on the performance of MWCNT ionic diode. Three MWCNT ionic diodes with ion channel lengths of 50, 100, and 150 μm , denoted by D_1 , D_2 , and D_3 , were readily fabricated on the same chip, by cutting the same bundle of MWCNTs into three segments of different lengths (Figure 2e and Figure S8a, Supporting Information). The mechanical avulsion method ensures the accurate control of the MWCNT nanochannel length, and the MWCNT nanochannels of the three diodes on the same chip possess consistent cross-section areas as they are made from the same bundle of MWCNTs. The four microchannels shown in Figure 2e were filled with 1% PDAC and 1% PSS in 1×10^{-3} M KCl solutions alternatively to modify the MWCNT terminals. Figure 2f shows the experimental results of the I – V curves measured from the three diodes and the corresponding rectification ratios of these diodes working at bias voltages of ± 5 V. One can observe that the forward current increases with decreasing channel length which is primarily due to the lower electric resistance of shorter ion channel while the reverse current keeps almost constant due to effective gating of co-ions at the channel entrances (Figure 2f). From the inset histogram of Figure 2f one can see that the ion current rectification ratio of these three diodes decreases from 39.8 ± 15.9 to 4.6 ± 1.2 ($n = 6$ for both) as the channel length increases from 50 to 150 μm . The rectification ratios of the diodes working at higher bias voltages of ± 7 V are summarized in Figure S8b in the Supporting Information, showing a similar decreasing trend with ion channel length as mentioned above.

The channel length effect was also investigated by numerical simulations (Section 1, Supporting Information) where the channel entrances were modified with charges of a limited charge modification length of 5 nm. The results demonstrated in Figure S8c in the Supporting Information show that the current rectification ratio increases with the channel length when the channel is shorter than ≈ 200 nm, while the ion current rectification ratio decreases with increasing channel length when the channel length is longer than ≈ 200 nm. The increase of ion current rectification ratio in the short-channel range can be explained by the entrance effects which dominate the current rectification behavior in nanopore-based ionic diodes,^[59] and the decrease of ion current rectification ratio with increasing channel length is assumed to be caused by the lower driven electric field on an ionic diode with longer ion channels. Generally, immobile charges decorated on the channel entrances repel co-ions effectively with very low leakage current when a reverse electric field is applied due to the strong electrostatic repulsion forces and the energy barrier; however, when a forward electric field is applied on the ion channel, promotion of counter-ions at the channel entrances happens and the degree of enrichment of counter-ions in the ion channel increases with the

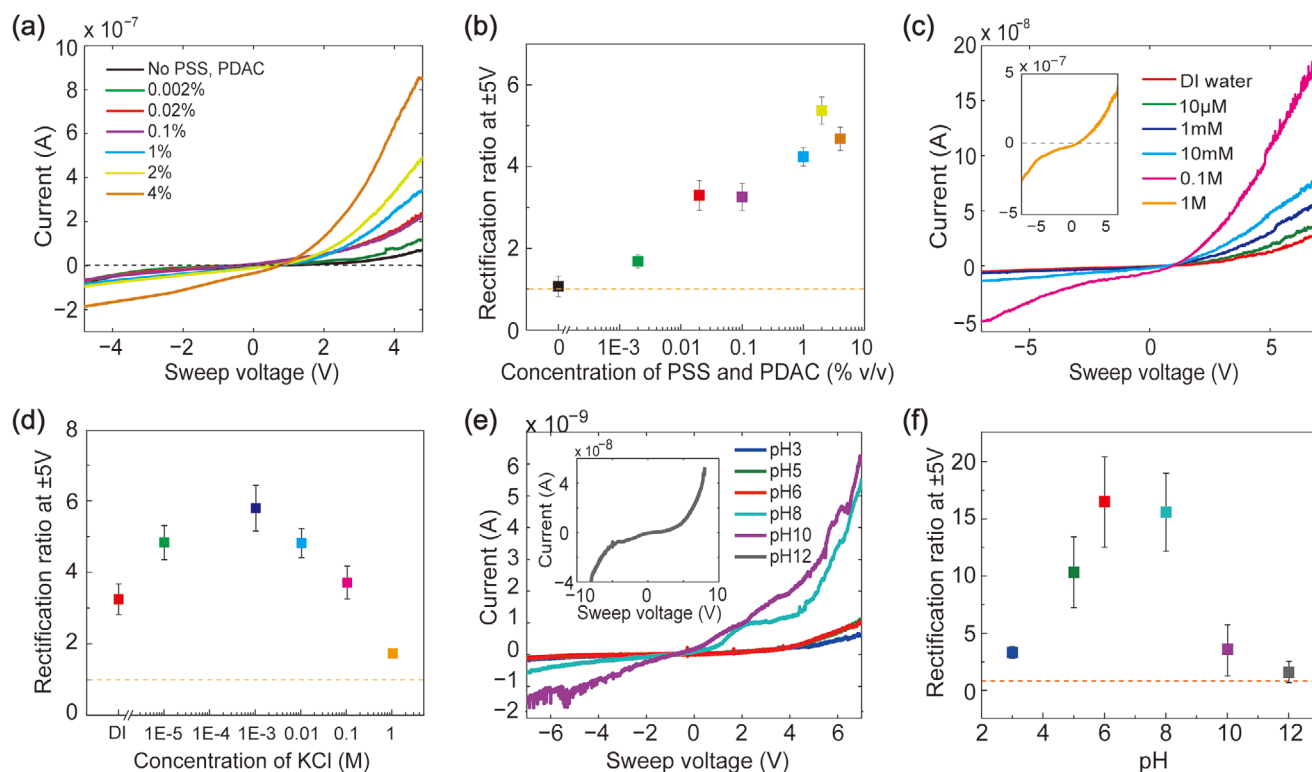


Figure 3. Experimental investigation of effects of working fluid conditions on the ionic diode performance. a,b) The effect of the polyelectrolyte concentration. For each experimentally measured I - V curve, PSS and PDAC were diluted in 1×10^{-3} M KCl solution (pH7) to the same concentration. c,d) The effect of the KCl concentration. All KCl solutions (pH7) contained 1% PDAC or 1% PSS. e,f) The effect of pH level of the KCl solutions. The channels were filled with 1×10^{-3} M KCl solution containing 1% PDAC or 1% PSS. The orange dashed lines indicate the rectification ratio of 1.

forward driven electric field. When a constant electric voltage is applied on the MWCNT diode, for a shorter ion channel, the driven electric field will be higher, thus giving rise to a higher degree of ion accumulation in the ion channel and a higher current rectification ratio, as shown in Figure 2f and Figure S8c in the Supporting Information, which is also consistent with numerical simulation results reported in the literature.^[59]

The shortest channel studied in the experiments was limited to 50 μ m. To further investigate the changing trend of the rectification ratio with the ion channel length in the nanometer range, we performed numerical simulations of MWCNT ionic diodes with ion channels of 5 nm in diameter and 10–500 nm in length. As shown in Figure S8c in the Supporting Information, the numerical simulation results show that, under a critical value of the ion channel length (240 nm under our simulation condition), the rectification ratio decreases with the ion channel length. This is because the interplay of the Debye length and the polarization effect at the nanochannel entrances.^[14,59] Therefore, for the current design of MWCNT ionic diodes, a short ion channel is beneficial for enhancing the current rectification effect. However, the current microfabrication technique limits the shortest length of the MWCNT ion channel that can be reliably constructed to be at the micrometer level. If the ion channel length is not limited by the device fabrication process, one should try to tune the ion channel length to this critical value to achieve the maximum rectification ratio of the ionic diode.

2.2.2. Effect of Ionic Conditions

The rectification effect of the MWCNT ionic diode is dominated by the electrostatic interactions between the charged MWCNT terminals and the mobile ions (K^+ and Cl^-), and the charge modification of the MWCNT terminals is mainly affected by concentrations of the two polyelectrolytes and pH levels of the KCl solutions in the upstream and downstream microchannels of the ionic diode. As a result, three key parameters were investigated to further understand the effect of the ionic conditions, including the polyelectrolyte concentration, the ionic concentration, and the pH level of the KCl solutions.

To study the effect of the polyelectrolyte concentration on the rectification performance of the MWCNT ionic diode, the MWCNT nanochannels (length: 100 μ m) were modified with PDAC on one terminal and PSS on the other terminal of the same v/v concentration ranging from 0.002% to 4% in 1×10^{-3} M KCl solution (pH7). As shown in Figure 3a, the measured I - V curves of ionic diodes with different polyelectrolyte concentrations confirm that the electric current of the diode increases with the polyelectrolyte concentration, which is caused by the stronger interactions between the MWCNT terminals and the mobile ions as well as the increasing concentrations of intrinsic mobile ions (Cl^- for PDAC and Na^+ for PSS) in the upstream and downstream solutions. Figure 3b summarizes the rectification ratios calculated from the I - V curves at ± 5 V, showing an increase of the rectification ratio from 1.1 ± 0.2 to 4.7 ± 0.3

($n = 5$ for both) with polyelectrolyte concentration increasing from 0% to 2%. Obviously, a higher polyelectrolyte concentration leads to a higher charge density at the MWCNT terminals and thus a higher level of ionic flux gating or enhancement at the nanochannel entrances. Note it is challenging to experimentally quantify the charge density at the MWCNT terminals. However, through numerical simulations, we proved that a higher charge density on the MWCNT terminals gives rise to a higher rectification ratio of the ionic diode (Figure S9a, Supporting Information), which qualitatively supports the experimental results shown in Figure 3b. However, in real operations of the MWCNT ionic diode, the polyelectrolyte concentration cannot be adjusted too high because it is hard to infuse highly viscous, high-concentration polyelectrolyte solutions into the upstream and downstream microchannels by pressure. For example, we found that, when injecting the 4% polyelectrolyte solutions, it was likely to cause leakage of the nanofluidic device under high injection pressure.

The ionotronic devices always need certain amount of charge carriers to work properly. During our experiments, KCl solutions of 10×10^{-6} M to 1 M containing 1% polyelectrolytes were injected into the same device from low to high concentrations sequentially, and the I - V curves (Figure 3c) and corresponding rectification ratios at ± 5 V (Figure 3d) and ± 7 V (Figure S9c, Supporting Information) were measured at different KCl concentrations. From Figure 3c, one can see that the ionic current increases with the KCl concentration because a higher KCl concentration provides more charge carriers in the ionic diode during operation. However, the rectification ratio, as shown in Figure 3d, first increases and then decreases with the KCl concentration, and the maximum of the rectification ratio occurs at the KCl concentration of 1×10^{-3} M. When the KCl concentration reaches as high as 1 M, the measured current rectification ratio of the diode reduces to, 1.7 ± 0.1 ($n = 5$).

This phenomenon can be explained by the electric double layer (EDL) theory^[60] and our numerical simulations (Figure S9b, Supporting Information). Theoretically, the thickness of EDL is 3–5 times of the Debye length (λ_D), which can be simplified as $\lambda_D = \frac{3.04}{z\sqrt{M}} \times 10^{-10}$ (m) for symmetrical electrolyte systems such as KCl solution,^[60] where M is the molarity of the symmetrical electrolyte solution, and z is the valence of the electrolyte. When the KCl concentration is as high as 1 M, the thickness of EDL near the MWCNT terminals becomes extremely thin ($\lambda_D \approx 1$ nm), and the immobilized charges on the MWCNT terminals are screened. As a result, there are little electrostatic gating of the mobile charges at the MWCNT terminals, giving rise to a low simulated charge rectification ratio of 1.03 at 1 M KCl in Figure S9b in the Supporting Information. This is consistent with the measured rectification ratio demonstrated in Figure 3d. However, the rectification ratio stops increasing at lower KCl concentrations in our experiments, which was also observed in conical-shaped ionic diodes.^[61] This is because the high-concentration polyelectrolytes release large amounts of Cl^- (from PDAC) and Na^+ (from PSS) to the solutions, giving rise to higher ionic strengths of the working solutions and thus thinner EDLs and weaker gating effect at the channel entrances.

The effect of pH level of the KCl solutions on the diode rectification performance has been investigated extensively on various designs,^[38,62–68] such as conical nanopores^[62,63] and straight nanochannels^[64,66] with bipolar or unipolar charge modifications. For our new design of the MWCNT ionic diode, we adjusted the pH level of the KCl solutions (1×10^{-3} M KCl with 1% polyelectrolytes) in the range of 3–12, and measured the I - V curves of the ionic diodes at different pH levels. As shown in Figure 3e, the ionic current increases with the pH level, which was similar to the results reported for other ionic diode platforms.^[63–65] The rectification ratio data shown in Figure 3f and Figure S9d in the Supporting Information reveal that the rectification effect of the MWCNT ionic diode reaches its maximum in the pH range of 6–8, and both strong acidic and strong basic environments cause significant reduction of the rectification ratio. This observation is in agreement with previously reported data.^[61] When polyelectrolytes are dissolved in water, expanded conformation of molecule chains occurs due to electrostatic repulsion between neighboring charged molecule chains and side groups.^[69] The expanded conformation of charged molecule chains at the MWCNT nanochannel terminals is favorable to the gating of co-ions and promotion of counter-ions through nanochannels. However, when the solution pH level is too high or too low, the additional H^+ and OH^- ions screen the charged groups on the MWCNT terminals and reduce the repulsion forces between the conformational chains;^[69] consequently, the gating or promotion of the ion transport through the nanochannels is significantly weakened and the rectification ratio is greatly reduced (as shown in Figure 3f and Figure S9d, Supporting Information). Based on the above results, one can conclude that for operating the MWCNT ionic diode, the working fluids should have a proper ionic concentration around 1×10^{-3} M and a neutral pH value.

2.3. Demonstration of MWCNT Ionic Electronic Circuits

After fully characterizing the rectification performance of the single MWCNT ionic diodes, we took advantage of the proposed microfabrication process for chip-scale integration of multiple MWCNT diodes to demonstrate monolithic ionic circuits such as ionic logic gates, rectifiers, and IBJT.

2.3.1. MWCNT Ionic Logic Circuits

Several logic gates have been demonstrated based on ionic diodes;^[10–12,70] however, these logic gate circuits are realized by connecting individual ionic diodes created on separate chips.^[11,12,70] Even though some efforts have been spent on integrating multiple ionic diodes on the same microfluidic chip for logic computing,^[10] there are still few examples of real-time logic processing demonstrated on such devices. Figure 4a illustrates the design of an “AND” gate based on two back-to-back connected MWCNT ionic diodes (NPN connection) formed by the configuration of PDAC–PSS–PDAC, in which the P and N terminals of the MWCNTs were modified with 1×10^{-3} M KCl solution of pH7 containing 1% polyelectrolytes, respectively. The AND gate was powered by a constant V_{cc} of 5 V applied through two resistors connected in series:

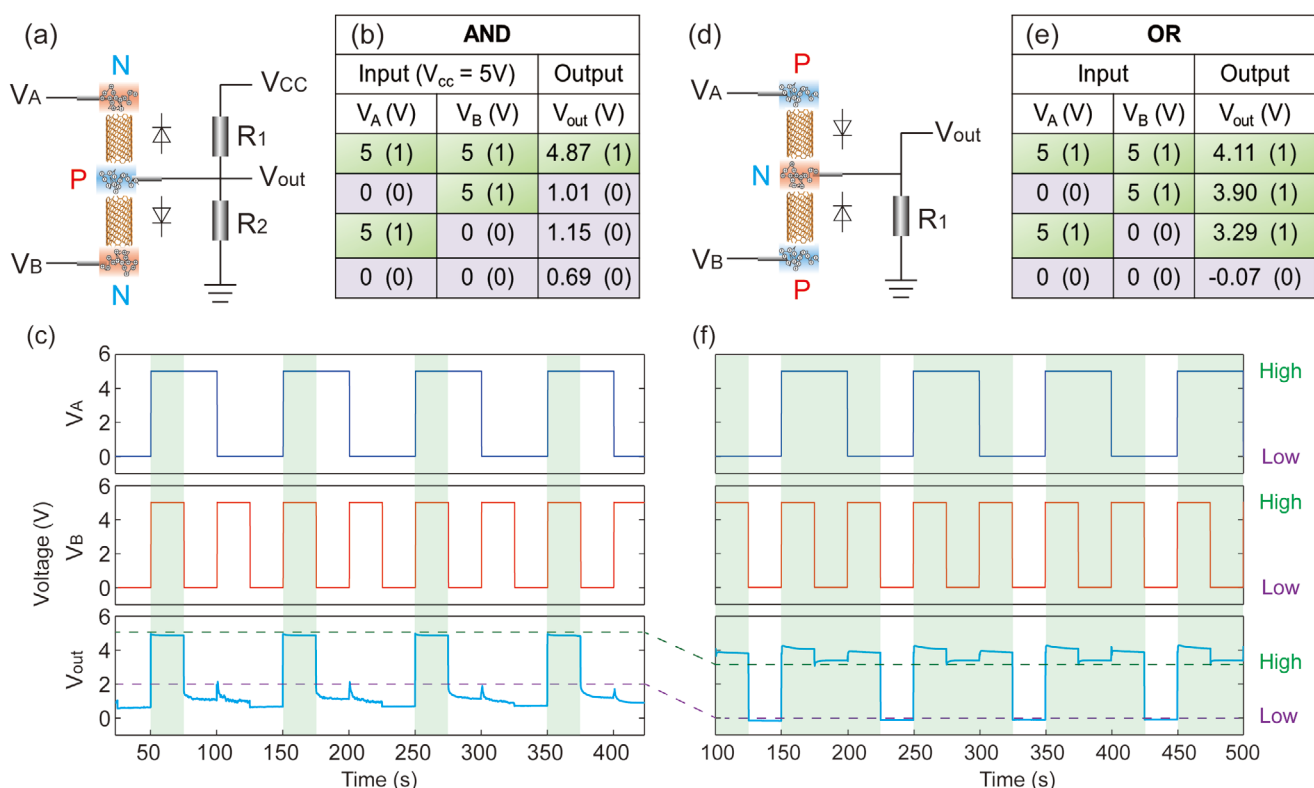


Figure 4. Demonstration of monolithic ionic logic gates (“AND” and “OR”) integrating two MWCNT ionic diodes. a) Schematic of an “AND” gate fabricated by two NPN-connected MWCNT ionic diodes. The resistors R_1 and R_2 are 500 M Ω and 5 G Ω , respectively. b) Truth table and c) experimental data of the input and output signals of the “AND” gate. d) Schematic of an “OR” gate fabricated by two PNP-connected MWCNT ionic diodes, where R_1 is 5 G Ω . e) Truth table and f) experimental data of the input and output signals of the “OR” logic gate.

$R_1 = 500$ M Ω and $R_2 = 5$ G Ω . The two input voltage signals V_A and V_B were applied on the two N terminals of the gate, and the voltage on the P terminal V_{out} served as the output signal of the gate. Figure S10a in the Supporting Information shows the picture of the ionic AND gate device. Figure 4b shows the truth table of the “AND” gate, where the light green background and the bracketed binary number “1” stand for the “high” status of the input/output signal, and the light purple background and the bracketed binary number “0” stand for the “low” status, while the values in the truth table give the analog values of the input (V_A and V_B) and output (V_{out}) voltages. Obviously, only in the first case, two “high” input signals (5 V) give the “high” output voltage (4.87 V). All the other three cases give “low” outputs of ≤ 1.15 V. The input and output signals of the AND gate were experimentally measured, as shown in Figure 4c, where the regions with light green background indicate the output at the “high” status. Note that there are small peaks and drifts at the “low” status, which are attributed to the I – V characteristic inconsistency between the two PN junctions and the charging and discharging-caused delays of the PN junctions. The input/output data in Figure 4c confirm that the ionic “AND” gate works properly and is more stable than the one made from nanomembrane-based ionic diodes reported recently.^[71]

Similarly, an ionic “OR” gate was integrated based on a PNP connection of two MWCNT ionic diodes (Figure 4d and Figure S10b, Supporting Information), where V_A and V_B are input signals and V_{out} is the output signal. Note that the

configuration of PNP connection can be obtained by simply changing the polarities of the above mentioned NPN connection via replacing the polyelectrolyte solutions in the microchannels with opposite charged polyelectrolyte to the configuration of PSS–PDAC–PSS. Figure 4e summarizes the measured truth table, suggesting a clear “OR” operation. Figure 4f shows the measured input/output voltage curves. Again, the small variations of the output voltage in its “high” status were caused by the slight inconsistency of the two PN junctions. We believe that the performance of these integrated ionic logic gates can be further improved by optimizing the characteristic consistency of the MWCNT ionic diodes in the same gate.

2.3.2. MWCNT Ionic Rectifier

Rectifiers are usually applied to convert AC signals to DC signals. A typical full-wave rectifier is usually constructed based on a four-diode bridge circuit, and the four-diode configuration ensures that the output current goes only in one direction regardless the polarity of the input signal. Inspired by the conventional rectifier, an ionic rectifier circuit consisting of four MWCNT ionic diodes was designed and integrated on a single MWCNT nanofluidic chip. The four MWCNT diodes were fabricated from the same bundle of MWCNTs, as shown in Figure 5a. The terminals of the MWCNT channels were modified with PDAC or PSS solutions alternatingly through

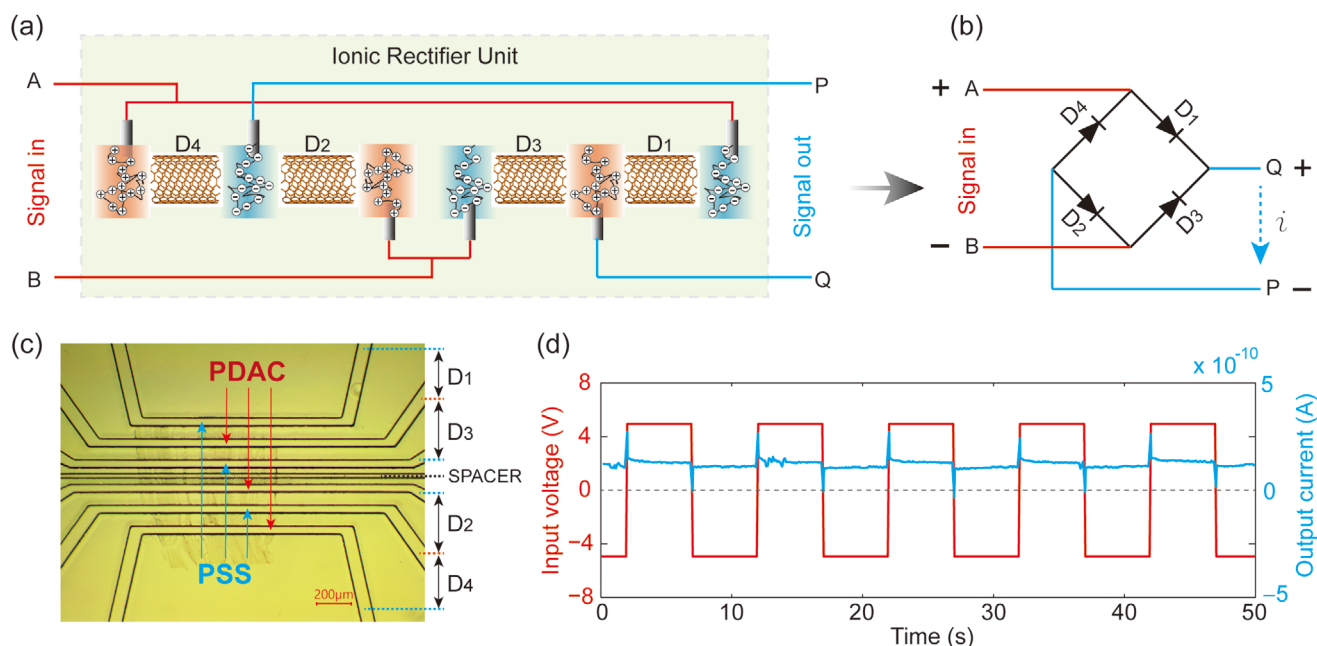


Figure 5. Demonstration of a monolithic MWCNT ionic rectifier. a) Schematic of an ionic rectifier integrating four MWCNT ionic diodes fabricated from the same bundle of long MWCNTs. b) Equivalent electric circuit of the MWCNT ionic rectifier. c) An optical image of the ionic rectifier. d) Rectification of 0.1 Hz square wave by the MWCNT ionic rectifier.

six microchannels to achieve the configuration of four diodes D_1 – D_4 . The corresponding schematic diagram of the rectifier circuit is shown in Figure 5b. Input signals were applied to the ionic rectifier through terminals A and B, and output signals were acquired through terminals P and Q. An optical image of the four ionic diodes fabricated on a silicon substrate is shown in Figure 5c, and photographs of the packaged nanofluidic device are shown in Figure S11a,b in the Supporting Information. The six working microchannels (50 μm wide and 60 μm high) were filled with 1×10^{-3} M KCl solutions (pH7), containing 1% polyelectrolytes, while the middle channel was left vacant as a spacer to prevent intermingling of solutions from the neighboring microchannels designed for D_2 and D_3 . The characterization of the ionic rectifier was conducted by applying a square-wave voltage to terminals A and B using a function generator and measuring the output current from terminals P and Q using a source meter, and all the electrical terminals were connected through Pt wires inserted into the corresponding microchannel reservoirs (Figure S11c, Supporting Information).

Figure 5e shows the experimental results of rectifying 0.1 Hz square wave with an amplitude of 5 V by a MWCNT ionic rectifier, and the real-time rectification process was recorded in Movie S1 in the Supporting Information. One can see that the output current remains relatively constant at a positive average value regardless of the polarity of the input voltage, showing a typical full-bridge rectifier characteristic. However, it should be mentioned that the rectified output current is at 0.1 nA level without any electrical load connected, which is because of the G Ω -level resistance of each ionic diode and the bias voltage of ± 5 V. The high internal resistance of the ionic diode is caused by the high aspect ratio ($\approx 70 \mu\text{m}/5 \text{ nm} = 14000$) of each MWCNT nanochannel and the limited number of ionic nanochannels in each diode. The resistance of each ionic diode can

be significantly lowered by reducing the length and increasing the number of the MWCNT nanochannels arranged in parallel. In addition, based on our testing results of the diode's frequency response (Figure 2b,c and Figure S6b–f, Supporting Information), the MWCNT ionic diode works more efficiently at lower frequencies because the mobile ions cannot response to the high-frequency alternations of the electric field.^[26] Consequently, the MWCNT ionic rectifier presented here is only suitable for low-frequency applications.

The performance consistency of different NWCNT ionic diodes is also essential to the proper operation of the ionic rectifier, which is mostly affected by diode-to-diode variations of the MWCNT morphology and terminal charge modification. As a result, in order to take full use of the proposed ionic rectifier, one has to pay attention to the following measures: i) shortening the length of MWCNT channels, ii) improving the uniformity of the MWCNT morphology, and iii) optimizing the charge modification process of the MWCNT terminals. Our approach of fabricating all the four ionic diodes from the same bundle of MWCNTs could significantly improve the MWCNT morphology uniformity of the diodes.

2.3.3. Demonstration of MWCNT IBJT

A traditional bipolar junction transistor is generally made up of two PN junctions and three terminals in which the current between two terminals can be modulated by the third one. Based on the polarity of the two PN junctions, PNP or NPN transistors are expected. Inspired by this configuration, an IBJT with two back-to-back ionic diodes was designed and created on a nanofluidic device. The top schematic in Figure 6a illustrates the layout of an NPN-type IBJT constructed from

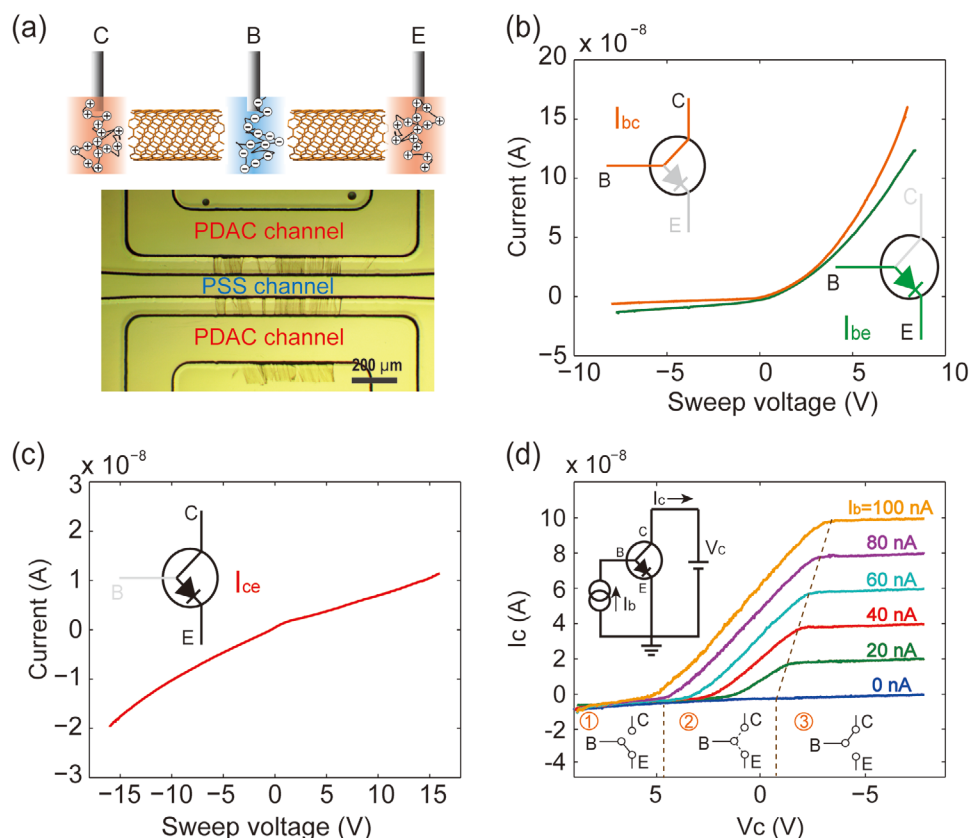


Figure 6. Demonstration of a monolithic MWCNT IBJT. a) Schematic (top) and optical image (bottom) of an NPN-type IBJT fabricated from the same bundle of MWCNTs. I - V characteristics of a MWCNT IBJT measured across terminals: b) BC and BE and c) CE. d) Diagram and testing results of an ionic switch circuit based on an IBJT working with 1×10^{-3} M KCl solution (pH7) containing 1% PDAC or PSS. The top-left diagram shows the ionic switch circuit and the three bottom insets illustrate three working conditions of the ionic switch.

the same bundle of MWCNTs, with its three terminals, C (Collector), B (Base) and E (Emitter) modified with polyelectrolytes. The bottom image in Figure 6a shows the configuration of the NPN-type IBJT. The experimental setup and an SEM image of the device can be found in Figure S12a,b in the Supporting Information. During our experiments, the microchannels were filled with 1×10^{-3} M KCl solution (pH7) containing 1% PDAC or PSS polyelectrolytes in the sequence of PDAC–PSS–PDAC to achieve the NPN configuration. Note that reconfiguration of a PNP-type IBJT can be obtained, if needed, by simply changing the polarities of PN junctions via replacing the polyelectrolyte solutions in the microchannels as mentioned above.

Figure 6b demonstrates I - V curves of both PN junctions between terminals B, C and terminals B, E of the NPN-type IBJT in the scanning range of -8 to 8 V, denoted by I_{bc} and I_{be} . Apparently, both PN junctions work with proper rectification operations. The slightly discrepancy between the two I - V curves is assumed to be caused by the inconsistency of the two PN junctions in terms of total number of MWCNTs and charge modification on the MWCNT terminals et al. Figure 6c demonstrates an I - V curve between terminals C and E, I_{ce} , with doubled scanning range between -16 and 16 V, showing no apparent “ON” and “OFF” status. The slightly leakage current around 20 nA at ± 16 V applied voltages is caused by the failure of fully turning off one of the PN junctions at the

reverse bias; however, the leakage current is much smaller than the “ON” status currents through terminals B, C and terminals B, E under the condition of 8 V forward applied bias which are around 150 nA, as shown in Figure 6b,c. The three I - V curves indicate that the two PN junctions in the NPN configuration operate normally.

As mentioned above, for an IBJT, the “ON” and “OFF” status between every two terminals are expected to be modulated by the third one.^[52] Figure 6d illustrates the experimental results of an ionic switch developed based on the NPN-type IBJT in which the top-left inset shows the equivalent electric circuit. An electric current I_b is injected to terminal B, and the current flow can be directed to terminal C or E by adjusting the electric potential on terminal C, V_c . Based on the amplitude and polarity of V_c , there are three cases as shown in the bottom insets in Figure 6d. For example, in regime 1) when a high positive bias V_c is applied on terminal C, the current through terminals C and E, I_c , is extremely low regardless of the injection current to terminal B, I_b . Based on the Kirchhoff’s current law, $I_b = I_c + I_e$, one can get that ionic current is essentially directed to terminal E, as a result, at regime 1), the nanofluidic junction between terminals B and E is “ON” while the ion channel between terminals B and C is “OFF”. However, in regime 3) when a high negative voltage V_c is applied on terminal C, ionic current from terminal B is directed to

terminal C, I_c is almost identical to the injection current I_b . Consequently, the ion channel between terminals B and E is “OFF” and the ion channel between terminals B and C is “ON” based on the Kirchhoff’s current law. Interestingly, in regime 2), the injection current from terminal B flows to both terminals E and C. In this transition regime, the proportion of the ionic current flow to terminal E or C can be modulated by V_c . Similarly, when a fixed electric bias V_c is applied between terminals C and E, the current through terminal C, I_c , can also be modulated by adjusting the bias on terminal B, as demonstrated in Figure S12c in the Supporting Information. As a result, the IBJT system can serve as a single-pole, double-throw ionic switch for regulation of ion transport. However, it is hard to create an ionic amplifier based on the IBJT because the base region is too large and the mobility of charge carriers (cations and anions) is too low.^[52] The operation of “ON” or “OFF” status of the ionic switch or desirable ion transport through ion channels tuned by the applied bias on the device terminals is potential for developing more advanced ionotronic systems such as for ion delivery.

3. Conclusions

In summary, this paper reports the design and circuit applications of a novel ionic diode developed on polyelectrolyte-brushed horizontally aligned MWCNTs, where ion transport through MWCNT channels was effectively regulated by oppositely charged polyelectrolytes brushed on the channel terminals. The working parameters of MWCNT ionic diode were systematically investigated by evaluating the ionic current rectification ratio. We showed that the current rectification ratio increased with concentration of polyelectrolytes, and MWCNT ionic diode worked properly with ionic concentration around 1×10^{-3} M of neutral pH condition. Reconfiguration of the polarity of MWCNT ionic diode can be achieved by reversely modifying the MWCNT terminals with oppositely charged polyelectrolytes. Through numerical simulations and experimental testing, we also revealed that the performance of MWCNT ionic systems can be optimized by shortening the length of MWCNT ion channels. Due to the intrinsic properties of ionic charge carriers, MWCNT ionic diodes can only operate properly at low frequency range. Enabled by the new batch fabrication process, multiple MWCNT ionic diodes can be integrated on a single nanofluidic chip to realize integrated ionotronic systems. We demonstrated the integration of ionic logic gates, ionic rectifiers and IBJT on single nanofluidic devices, which highlights the promise of our MWCNT ionic diode design for constructing monolithic ionotronic systems with many diode and transistor components. The development of the MWCNT nanofluidic devices may also provide powerful platforms for fundamental research of electrokinetic transport behavior in nanochannels and functionalities of 1D carbon materials. We believe that the proposed MWCNT ionotronic systems may open a new paradigm to a wide range of new applications, such as mimicking ionic related biological systems, controlling delivery of ionic species, and developing advanced ionotronic intelligent devices.

4. Experimental Section

Synthesis and Characterization of MWCNTs: Vertically aligned MWCNT forests (Figure 1c) were synthesized on Si/SiO₂ substrates by CVD.^[72,73] An iron (Fe) layer (≈ 4 nm thick) was deposited on the wafers by electron-beam evaporation (inset of Figure S2h in the Supporting Information) to work as the catalyst. Patterning of the Fe catalyst film was carried out by standard photolithography followed by lift-off (see Section 2 in the Supporting Information for the details). Vertically aligned MWCNTs were grown on the catalyst by using the CVD method at a temperature of 725 °C. During the synthesis, ethylene together with argon and hydrogen (70:70:70 sccm) were mixed in a furnace tube (25 mm in diameter, Lindberg) to supply the carbon source. The in-plane length and width of the MWCNT forest patterns were defined by the size of the Fe film patterns and the height of the MWCNTs was controlled by the growth time between 30–60 min, and MWCNTs from 500 μ m to 1 mm in length were used in this study. The diameter of the MWCNTs was characterized by TEM (Figure S2h,i, Supporting Information), showing the MWCNTs contain 10–15 layers with a smooth inner diameter of around 5 nm, as shown in Figure S2i in the Supporting Information. The distribution of the inner diameter of MWCNTs was obtained by measuring the MWCNT array at different locations ($n = 54$) by TEM and fitted by a Gaussian curve. The quality of MWCNTs was also examined by Raman spectroscopy, showing clear D-band, G-band, and 2D-band peaking at 1350, 1583, and 2678 cm^{-1} , respectively (Figure S2j, Supporting Information). MWCNT terminals after mechanical avulsion were observed by SEM. The samples were prepared by cutting Si-based nanofluidic chip with a diamond tip. Figure S2e in the Supporting Information shows an example of the sample where the red arrow indicates the SEM scanning area. The cross-section of the MWCNTs after avulsion is shown in Figure S2f in the Supporting Information, and a zoomed-in view is demonstrated in Figure S2g in the Supporting Information.

Fabrication of MWCNT Nanofluidic Chips: The nanofluidic chip was composed of two layers, the top layer was a thick layer of PDMS (≈ 2.5 mm) prepared by curing a mixture of curing reagent and polymer base (1:10) in an oven at 80 °C for 2 h followed by punching channel reservoirs. The bottom layer with MWCNT channels was fabricated by following the working procedure reported in the reference^[21] as well demonstrated in Figure 1f and Figure S2a–d in the Supporting Information. Briefly, a thin layer of SU8 photoresist (5 μ m) was spin coated on a Si wafer with an oxidized insulation layer (300 nm SiO₂). Thereafter, a bundle of horizontally aligned MWCNTs (Figure S2a, Supporting Information) exfoliated from a MWCNT forest was transferred on the photoresist-coated wafer, followed by spin coating another layer of thick photoresist (50 μ m) to embed the MWCNTs (Figure 1f–I). A photolithography protocol including UV exposure (Figure S2b, Supporting Information and Figure 1f–II) and wet development (Figure S2c, Supporting Information and Figure 1f–III) was applied to pattern microchannels on the photoresist layer in which the MWCNTs bridge the microchannels. Residual MWCNTs in the microchannels were removed by mechanical avulsion with the aid of PDMS casting, as illustrated in Figure 1f–IV. Figure 1g and Figure S2d,m in the Supporting Information show examples of chips after avulsion of MWCNTs. The mechanical avulsion method was proved more effective than the conventionally used oxygen plasma etching method (Figure S2k–m, Supporting Information). The bottom layer with perfect trimmed MWCNT openings (Figure S2f, Supporting Information) and the top PDMS cover punched with channel reservoirs were bonded together by oxygen plasma activation (30 s) followed by heating at 85 °C for 30 min to enhance the bonding force (Figure 1f–V). The nanofluidic chip was sandwiched by two pieces of 5 mm thick PMMA slabs cut with channel wells and squeezed by bolts and nuts to avoid any potential leakage. Working solutions were loaded into microchannels followed by incubation at room temperature for 30 min to allow fully absorption of polycations and polyanions on the MWCNT terminals. To verify the absorption of polyelectrolyte on MWCNTs, energy-dispersive X-ray spectroscopy (EDX) was applied to detect the elements of polyelectrolyte-modified MWCNTs after washing

by DI water. The results indicate that absorption of polyelectrolytes on MWCNTs was hard to be completely removed by simple washing (Figure S3, Supporting Information), which coincides with the wash cycle test conducted on an ionic diode (Figure S5a, Supporting Information).

Chemical Reagents and Instruments: KCl solution was prepared by dissolving KCl powder (Fisher Scientific) into DI water. Original PDAC (Mw \approx 400 000, 20 wt% in water, Sigma Aldrich) solution and PSS (Mw \approx 7 000 000, 30 wt% in water, Sigma Aldrich) solution were diluted in KCl solutions before modification of MWCNTs. PDMS precursor (Sylgard 184) was prepared by mixing PDMS base with curing agent (w/w ratio: 10:1). Photomasks for photolithography were designed by AutoCAD and printed at a resolution of 5 μ m (CAD/Art Services, Inc.). Nanofluidic chips were fabricated on Silicon wafers (University Wafer) thermally oxidized with 300 nm SiO₂ insulation layers (Bruce Technologies Oxidation Furnace). SU-8 2005, SU-8 2075 photoresists (MicroChem), and SU-8 developer were applied in the photolithography protocols. Plasma (Harrick plasma, PDC-32G) and corona treatment (Corona SB, SoftLithoBox) were used in the chip activation and bonding process. Oxygen plasma etching of MWCNTs was conducted by plasma asher (TePla Technics 100-E). Bundles of MWCNTs were isolated from MWCNT forests by scotch tape (3M) and characterized by optical microscopy (Motic, BA 310) installed with CCD camera (Optixcam, Summit K2), AFM (Hitachi, 5100N), SEM (Hitachi-SU3500, JEOL-6610LV and FEI Quanta FEG 250) and high-resolution transmission electron microscopy (HR-TEM, JEOL JEM-2010) as well as Raman spectroscopy (Horiba Jobin Yvon LabRam 800hR spectrometer with a synapse CCD detector). MWCNTs modified with polyelectrolytes were characterized by EDX (Oxford Instruments). Source meters (Keithley 6202, Keysight B2902A) and function generators (Agilent, 33220A) were applied for nanofluidic chips characterization through Pt electrodes (Sigma-Aldrich). A homemade Faraday case and shielding cables were applied during the experiments to minimize the surrounding noises. PDA Tubing (1/16" OD), microvalves (IDEX Health & Science) and laser cutter (Universal Laser Systems) patterned PMMA boards (McMaster-Carr) were applied to assemble the final devices. Numerical simulation of ionic diodes was conducted by Finite Element Analysis (FEA) on Comsol 5.3, as demonstrated in Section 1 in the Supporting Information.

Experimental Data Acquisition and Processing: Nanofluidic chips were initially filled with DI water containing 5% ethanol for 10 min to fully wet the MWCNT channels and remove chemical residuals in the microchannels. The pristine solution was replaced by polyelectrolyte solutions via syringe pumps thereafter. Before each test, the microchannels were flushed with 200 μ L fresh polyelectrolyte solutions to remove the residual solutions from the previous round testing for at least five times to reset the nanofluidic system. The chips never dried during the whole testing period to avoid failure of refilling and sedimentation of polyelectrolytes in the microchannels due to the evaporation of water. Electrical properties of ionic diodes, ionic rectifiers, and gate logic circuits were characterized by source meters and function generators. For I - V curve measurement, repeatedly bidirectional scanning (Figure S4a, Supporting Information) at 100 mV s⁻¹ was conducted through all the experiments. However, due to the intrinsic slow response properties of ion transport in aqueous solutions,^[52] there was a slight noncoincidence between the forward scanning and reverse scanning trajectories, as shown in Figure S4a in the Supporting Information, and a slight variation in the rectification ratio at different scanning speed (Figure S4b,c, Supporting Information). To minimize errors triggered by the scanning speed, the scanning speed was kept consistent at 100 mV s⁻¹ through all the testing. To study the working fluid effects on the performance of chips, electrolyte solutions in the microchannels changed gradually from low concentration to high concentration or low pH value to high pH value gradually. All the experiments were repeated on the same chip for at least three times and on different chips to assure the reproducibility of results at room temperature around 23 °C.

Supporting Information

Supporting Information is available from the Wiley Online Library or from the author.

Acknowledgements

The authors acknowledge the financial support from the Natural Sciences and Engineering Research Council of Canada (Grant #RGPIN-2017-06374, #RGPAS-2017-507980 and #DGDND-2017-00001), from the Canada Foundation for Innovation (Grant #JELF-37812). Acknowledgements are due to Dr. Li Yu and Binbin Ying for valuable discussions, Sina Kheiri for his assistance in figure rendering, and Peng Pan and Dr. Qigao Fan for their efforts in the electrical testing system troubleshooting.

Conflict of Interest

The authors declare no conflict of interest.

Keywords

ionic diodes, ionotronics, multiwalled carbon nanotubes, nanofluidics

Received: April 9, 2020

Revised: May 23, 2020

Published online: July 23, 2020

- [1] Z. Zhang, L. Wen, L. Jiang, *Chem. Soc. Rev.* **2018**, 47, 322.
- [2] X. Huang, X. Y. Kong, L. Wen, L. Jiang, *Adv. Funct. Mater.* **2018**, 28, 1801079.
- [3] H. Chun, T. D. Chung, *Annu. Rev. Anal. Chem.* **2015**, 8, 441.
- [4] Z. S. Siwy, M. R. Powell, A. Petrov, E. Kalman, C. Trautmann, R. S. Eisenberg, *Nano Lett.* **2006**, 6, 1729.
- [5] S. Majd, E. C. Yusko, Y. N. Billeh, M. X. Macrae, J. Yang, M. Mayer, *Curr. Opin. Biotechnol.* **2010**, 21, 439.
- [6] X. Hou, W. Guo, L. Jiang, *Chem. Soc. Rev.* **2011**, 40, 2385.
- [7] X. Strakosas, J. Selberg, Z. Hemmatian, M. Rolandi, *Adv. Sci.* **2017**, 4, 1600527.
- [8] P. Janson, E. O. Gabrielsson, K. J. Lee, M. Berggren, D. T. Simon, *Adv. Mater. Technol.* **2019**, 4, 1800494.
- [9] E. O. Gabrielsson, K. Tybrandt, M. Berggren, *Lab Chip* **2012**, 12, 2507.
- [10] J. H. Han, K. B. Kim, H. C. Kim, T. D. Chung, *Angew. Chem., Int. Ed.* **2009**, 48, 3830.
- [11] M. Ali, S. Mafe, P. Ramirez, R. Neumann, W. Ensinger, *Langmuir* **2009**, 25, 11993.
- [12] J. Cervera, P. Ramirez, S. Mafe, P. Stroeve, *Electrochim. Acta* **2011**, 56, 4504.
- [13] Y. Tian, L. Wen, X. Hou, G. Hou, L. Jiang, *ChemPhysChem* **2012**, 13, 2455.
- [14] I. Vlasiouk, T. R. Kozel, Z. S. Siwy, *J. Am. Chem. Soc.* **2009**, 131, 8211.
- [15] Y. Feng, W. Zhu, W. Guo, L. Jiang, *Adv. Mater.* **2017**, 29, 1702773.
- [16] K. Xiao, P. Giusto, L. Wen, L. Jiang, M. Antonietti, *Angew. Chem., Int. Ed.* **2018**, 57, 10123.
- [17] X. Hou, Z. S. Siwy, M. Ulbricht, *Small* **2018**, 14, 1800908.
- [18] X. Hou, H. Zhang, L. Jiang, *Angew. Chem., Int. Ed.* **2012**, 51, 5296.
- [19] S. Chen, Y. Tang, K. Zhan, D. Sun, X. Hou, *Nano Today* **2018**, 20, 84.
- [20] X. Hou, *Adv. Mater.* **2016**, 28, 7049.
- [21] R. Peng, X. S. Tang, D. Li, *Small* **2018**, 14, 1800013.

- [22] K. Xiao, L. Chen, Z. Zhang, G. Xie, P. Li, X. Y. Kong, L. Wen, L. Jiang, *Angew. Chem., Int. Ed.* **2017**, 56, 8168.
- [23] Y. Zhao, Y. Cai, L. Zhang, B. Li, G. Zhang, J. T. L. Thong, *Adv. Funct. Mater.* **2019**, 30, 1903929.
- [24] H. Zhang, Y. Tian, L. Jiang, *Nano Today* **2016**, 11, 61.
- [25] C. Duan, W. Wang, Q. Xie, *Biomechanics* **2013**, 7, 026501.
- [26] E. O. Gabrielson, P. Janson, K. Tybrandt, D. T. Simon, M. Berggren, *Adv. Mater.* **2014**, 26, 5143.
- [27] L. M. Peng, Z. Zhang, S. Wang, *Mater. Today* **2014**, 17, 433.
- [28] S. Hong, S. Myung, *Nat. Nanotechnol.* **2007**, 2, 207.
- [29] Q. Cao, J. Tersoff, D. B. Farmer, Y. Zhu, S. J. Han, *Science* **2017**, 356, 1369.
- [30] S. J. Han, J. Tang, B. Kumar, A. Falk, D. Farmer, G. Tulevski, K. Jenkins, A. Afzali, S. Oida, J. Ott, J. Hannon, W. Haensch, *Nat. Nanotechnol.* **2017**, 12, 861.
- [31] G. Hills, C. Lau, A. Wright, S. Fuller, M. D. Bishop, T. Srimani, P. Kanhaiya, R. Ho, A. Amer, Y. Stein, D. Murphy, Arvind, A. Chandrakasan, M. M. Shulaker, *Nature* **2019**, 572, 595.
- [32] R. Tunuguntla, R. Y. Henley, Y.-C. Yao, T. A. Pham, M. Wanunu, A. Noy, *Science* **2017**, 357, 792.
- [33] J. Geng, K. Kim, J. Zhang, A. Escalada, R. Tunuguntla, L. R. Comolli, F. I. Allen, A. V. Shnyrova, K. R. Cho, D. Munoz, Y. M. Wang, C. P. Grigoropoulos, C. M. Ajo-Franklin, V. A. Frolov, A. Noy, *Nature* **2014**, 514, 612.
- [34] B. A. G. Hummer, J. C. Rasaiah, J. P. Noworyta, *Nature* **2001**, 414, 188.
- [35] M. Wang, Z. Sheng, X. Hou, Y. Zhang, D. Wang, H. Meng, B. Chen, K. Zhan, Y. Yin, P. Stroeve, *Adv. Mater.* **2019**, 31, 1805130.
- [36] C. M. Q. Le, X. T. Cao, D. W. Kim, U. H. Ban, S. H. Lee, K. T. Lim, *Mol. Cryst. Liq. Cryst.* **2017**, 654, 181.
- [37] J. Wu, K. Gerstandt, H. Zhang, J. Liu, B. J. Hinds, *Nat. Nanotechnol.* **2012**, 7, 133.
- [38] F. Fornasiero, J. Bin In, S. Kim, H. G. Park, Y. Wang, C. P. Grigoropoulos, A. Noy, O. Bakajin, *Langmuir* **2010**, 26, 14848.
- [39] N. R. Scruggs, J. W. F. Robertson, J. J. Kasianowicz, K. B. Migler, *Nano Lett.* **2009**, 9, 3853.
- [40] H. Amiri, K. L. Shepard, C. Nuckolls, R. Hernández Sánchez, *Nano Lett.* **2017**, 17, 1204.
- [41] L. J. Cheng, L. J. Guo, *Chem. Soc. Rev.* **2010**, 39, 923.
- [42] S. E. Moya, A. Ilie, J. S. Bendall, J. L. Hernandez-Lopez, J. Ruiz-García, W. T. S. Huck, *Macromol. Chem. Phys.* **2007**, 208, 603.
- [43] M. Tagliazucchi, Y. Rabin, I. Szleifer, *ACS Nano* **2013**, 7, 9085.
- [44] T. Fukushima, T. Aida, *Chem. - Eur. J.* **2007**, 13, 5048.
- [45] J. Luceño Sánchez, R. Peña Capilla, A. Díez-Pascual, *Polymers* **2018**, 10, 1169.
- [46] V. Schroeder, S. Savagatrup, M. He, S. Lin, T. M. Swager, *Chem. Rev.* **2019**, 119, 599.
- [47] M. Mazloumi, S. Shadmehr, Y. Rangom, L. F. Nazar, X. S. Tang, *ACS Nano* **2013**, 7, 4281.
- [48] H. H. Liu, J. He, J. Tang, P. Pang, D. Cao, P. Krstic, S. Joseph, S. Lindsay, C. Nuckolls, H. H. Liu, P. Pang, D. Cao, P. Krstic, S. Joseph, S. Lindsay, C. Nuckolls, *Science* **2010**, 327, 64.
- [49] K. Xiao, G. Xie, Z. Zhang, X. Y. Kong, Q. Liu, P. Li, L. Wen, L. Jiang, *Adv. Mater.* **2016**, 28, 3345.
- [50] C. Zhao, J. Lu, J. Hou, X. Li, J. Wang, L. Jiang, H. Wang, H. Zhang, *Adv. Funct. Mater.* **2019**, 29, 1806416.
- [51] R. Peng, D. Li, *Nanoscale* **2016**, 8, 12237.
- [52] L. J. Cheng, L. J. Guo, *ACS Nano* **2009**, 3, 575.
- [53] M. Mainak, C. Nitin, A. Rodney, J. H. Bruce, *Nature* **2005**, 438, 43.
- [54] J. K. Holt, H. G. Park, Y. Wang, M. Stadermann, A. B. Artyukhin, C. P. Grigoropoulos, A. Noy, O. Bakajin, *Science* **2006**, 312, 1034.
- [55] M. Whitby, N. Quirke, *Nat. Nanotechnol.* **2007**, 2, 87.
- [56] B. Qiu, B. Lin, F. Yan, *Polym. Int.* **2013**, 62, 335.
- [57] Z. Zhang, X. Y. Kong, K. Xiao, Q. Liu, G. Xie, P. Li, J. Ma, Y. Tian, L. Wen, L. Jiang, *J. Am. Chem. Soc.* **2015**, 137, 14765.
- [58] I. Vlassiuk, S. Smimov, Z. Siwy, *ACS Nano* **2008**, 2, 1589.
- [59] Y. Ma, J. Guo, L. Jia, Y. Xie, *ACS Sens.* **2018**, 3, 167.
- [60] D. Li, *Electrokinetics in Microfluidics*, Vol. 2, Academic Press, Amsterdam **2004**.
- [61] I. Vlassiuk, Z. S. Siwy, *Nano Lett.* **2007**, 7, 552.
- [62] M. Ali, P. Ramirez, S. Mafé, R. Neumann, W. Ensinger, *ACS Nano* **2009**, 3, 603.
- [63] J. P. Hsu, H. H. Wu, C. Y. Lin, S. Tseng, *Anal. Chem.* **2017**, 89, 3952.
- [64] C. Y. Li, F. X. Ma, Z. Q. Wu, H. L. Gao, W. T. Shao, K. Wang, X. H. Xia, *Adv. Funct. Mater.* **2013**, 23, 3836.
- [65] C. Y. Lin, L. H. Yeh, Z. S. Siwy, *J. Phys. Chem. Lett.* **2018**, 9, 393.
- [66] Z. Meng, Y. Chen, X. Li, Y. Xu, J. Zhai, *ACS Appl. Mater. Interfaces* **2015**, 7, 7709.
- [67] P. Ramirez, V. Gomez, M. Ali, W. Ensinger, S. Mafe, *Electrochem. Commun.* **2013**, 31, 137.
- [68] N. Sa, L. A. Baker, *J. Am. Chem. Soc.* **2011**, 133, 10398.
- [69] G. Kocak, C. Tuncer, V. Bütün, *Polym. Chem.* **2017**, 8, 144.
- [70] H. Grebel, *Thin Solid Films* **2017**, 638, 138.
- [71] Y. Wang, Z. Wang, Z. Su, S. Cai, *Extreme Mech. Lett.* **2019**, 28, 81.
- [72] S. Shadmehr, M. Coleman, B. Liu, J. Liu, X. S. Tang, *RSC Adv.* **2017**, 7, 611.
- [73] S. R. Shin, C. Shin, A. Memic, S. Shadmehr, M. Miscuglio, H. Y. Jung, S. M. Jung, H. Bae, A. Khademhosseini, X. Tang, M. R. Dokmeci, *Adv. Funct. Mater.* **2015**, 25, 4486.